Proton NMR Investigation of the Heme Active Site Structure of an Engineered Cytochrome *c* Peroxidase that Mimics Manganese Peroxidase†

Xiaotang Wang and Yi Lu*

Department of Chemistry, University of Illinois at Urbana−Champaign, Urbana, Illinois 61801

Received February 1, 1999; Revised Manuscript Received May 11, 1999

ABSTRACT: The heme active site structure of an engineered cytochrome *c* peroxidase [MnC*c*P; see Yeung, B. K., et al. (1997) *Chem. Biol. 4*, 215−221] that closely mimics manganese peroxidase (MnP) has been characterized by both one- and two-dimensional NMR spectroscopy. All hyperfine-shifted resonances from the heme pocket as well as resonances from catalytically relevant amino acid residues in the congested diamagnetic envelope have been assigned. From the NMR spectral assignment and the line broadening pattern of specific protons in NOESY spectra of MnC*c*P, the location of the engineered Mn(II) center is firmly identified. Furthermore, we found that the creation of the Mn(II)-binding site in C*c*P resulted in no detectable structural changes on the distal heme pocket of the protein. However, notable structural changes are observed at the proximal side of the heme cavity. Both CϵH shift of the proximal histidine and ^{15}N shift of the bound C^{15}N$^-$ suggest a weaker heme Fe(III)−N(His) bond in MnC*c*P compared to WtC*c*P. Our results indicate that the engineered Mn(II)-binding site in C*c*P resulted in not only a similar Mn(II)-binding affinity and improved MnP activity, but also weakened the Fe(III)−N(His) bond strength of the template protein C*c*P so that its bond strength is similar to that of the target protein MnP. The results presented here help elucidate the impact of designing a metal-binding site on both the local and global structure of the enzyme, and provide a structural basis for engineering the next generation of MnC*c*P that mimics MnP more closely.

Peroxidases are a ubiquitous class of enzymes that catalyze the oxidation of a wide variety of organic and inorganic substrate molecules at the expense of hydrogen peroxide or other organic hydroperoxides (*1*−*4*). Most peroxidases contain an iron protoporphyrin IX moiety or heme *b* (Figure 1) as their prosthetic group and share common reaction intermediates (*1*). Detailed crystallographic studies on cytochrome *c* peroxidases (C*c*P)[1] (*5*−*7*), lignin peroxidase (LiP) (*8, 9*), manganese peroxidase (MnP) (*10*), and horseradish peroxidase (HRP)(*11*) have firmly established the similarity of the active site structure of these peroxidases. Despite this general similarity, the catalytic activities and biological functions of these peroxidases are quite diverse (*1*−*4*), ranging from the oxidation of small inorganic halides (chloroperoxidase) to the long-range electron transfer to large biomolecules such as cytochrome *c* (C*c*P). The functional diversity among heme peroxidases has been attributed to specific structural differences around the heme-binding site including the nature of the axial ligand and the environment of the substrate-binding sites (*1, 12*−*18*). Identifying the structural differences and understanding how these differences can modulate the functional properties of peroxidases should allow use of these enzymes more effectively in biotechnological applications.

Manganese peroxidase (MnP) is an extracellular heme peroxidase from the white-rot fungus *Phanerochaete chrysosporium* which can degrade both lignin, a complex phenylpropanoid polymer, and many xenobiotic compounds such as polychlorinated biphenyls (*19*−*21*). The structure and function relationships in MnP have received increasing attention in recent years because of its ability to degrade aromatic pollutants. It has been proposed that the key step in the biodegradatative function of MnP is the oxidation of Mn(II) to Mn(III) (*19*−*21*). Therefore, it is critical to gain thorough knowledge of the Mn(II)-binding site in MnP.

The Mn(II)-binding site in MnP has been investigated by many spectroscopic and X-ray crystallographic studies. UV−vis titrations have demonstrated the binding of one Mn(II) ion to each molecule of the protein (*22, 23*). Paramagnetic NMR studies showed that signals near the binding site are specifically broadened upon Mn(II) binding (*24*). The X-ray crystal structure of this peroxidase has revealed that the Mn(II)-binding site consists of two glutamates (Glu35, Glu39), one aspartate (Asp179), one heme propionate, and two water molecules (*10, 25*). Recently, site-directed mutagenesis

† This work is supported by National Science Foundation CHE 95-0242 (CAREER Award and Special Creativity Extension). Y.L. is a Sloan Research Fellow of the Alfred Sloan Foundation, a Cottrell Scholar of Research Corporation, a Camille Dreyfus Teacher−Scholar of the Camille and Henry Dreyfus Foundation, and a Beckman Young Investigator of the Arnold and Mabel Beckman Foundation.

* To whom correspondence should be addressed. Telephone: (217) 333-2619. FAX: (217) 333-2685. E-mail yi-lu@uiuc.edu.

[1] Abbreviations: NMR, nuclear magnetic resonance; NOE, nuclear Overhauser effect; NOESY, nuclear Overhauser enhancement spectroscopy; WtC*c*P, wild-type cytochrome *c* peroxidase; WtC*c*PCN, cyanide-bound low-spin form of WtC*c*P; MnC*c*P, cytochrome *c* peroxidase containing Gly41→Glu, Val45→Glu, and His181→Asp triple mutations; MnC*c*PCN, cyanide-ligated low-spin form of MnC*c*P; MnP, manganese peroxidase; MnPCN, cyanide-bound low-spin form of MnP; LiP, lignin peroxidase; LiPCN, cyanide-bound low-spin form of LiP; HRP, horseradish peroxidase; HRPCN, cyanide-bound low-spin form of HRP.

10.1021/bi990235r CCC: $18.00
Published on Web 06/19/1999

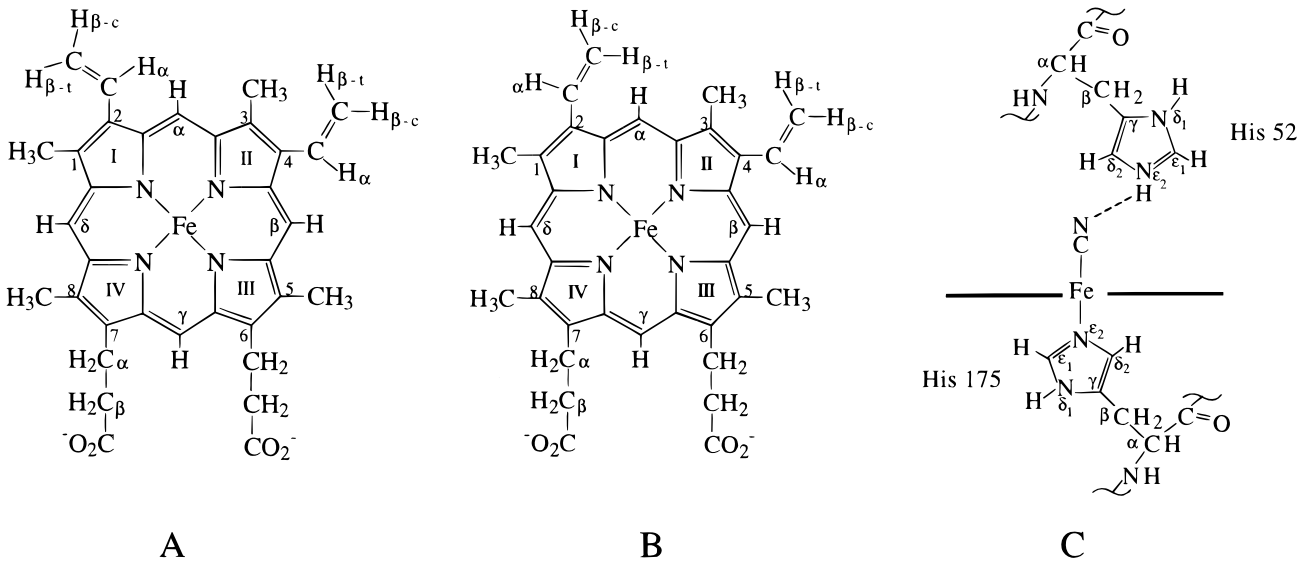

FIGURE 1: Schematic presentation of different conformations of iron protoporphyrin IX in peroxidases [(A) for C*c*P and MnP and (B) for HRP and LiP] and (C) the axial ligands of the heme iron for peroxidase−cyanide complexes showing the labeling scheme used in this work.

studies have been carried out on MnP, and the importance of each individual ligand to Mn(II) was clarified (*25*−*27*). The results from these studies contributed greatly to the understanding of the structure of the Mn(II)-binding site in MnP.

We are interested in investigating the key structural features of metalloenzymes and toward this goal we employ the protein redesign approach in our studies. Like *de novo* protein design (*28*), the protein redesign approach complements the biochemical, spectroscopic, and site-directed mutagenesis studies used to investigate structure and function relationships of native enzymes (*29*). Both *de novo* design and protein redesign are minimalistic approaches and can serve as touchstones whereby the knowledge about the structure and function of enzymes gained through the study of the native enzymes can be tested. They are capable of answering the question of whether the *necessary* structural features identified from study of native enzymes are *sufficient* to confer the structure and function of the enzymes. An advantage of the protein redesign approach to the study of the role of active sites such as Mn(II)-binding site in proteins lies in the fact that protein redesign builds on an existing protein scaffold. This is important since nature is known to use only a limited number of protein scaffoldings and yet is able to achieve diverse functions by redesigning the active site. In our studies, we have utilized C*c*P as one of our building blocks.

We have applied the protein redesign approach to investigate the role of the Mn(II)-binding site on MnP activity (*30*). In particular, we are interested in determining how the Mn(II)-binding site can be constructed in a peroxidase, and whether the Mn(II)-binding site alone will confer MnP activity in a peroxidase that does not have the MnP activity. C*c*P, a prototype heme peroxidase whose engineering, expression, spectroscopic, and X-ray crystallographic characterization has been well established (*3*, *4*, *31*), is an ideal template protein for such investigations. Despite the close similarities in the overall folding pattern and heme active site to that in MnP (*10*), C*c*P does not contain the Mn(II)-binding site and shows no MnP activity. In C*c*P, while the heme propionate oxygen is available for binding Mn(II), the amino acids corresponding to Glu35, Glu39, and Asp179 in MnP are Gly41, Val45, and His181, respectively. Since our template protein C*c*P is less than 25% homologous in sequence to our target protein MnP, the effect of an engineered Mn(II)-binding site on the ability of C*c*P to oxidize Mn(II) should provide insight into the relative importance of the Mn(II) site and other structural features for MnP activity.

We have reported our initial success in engineering a Mn(II)-binding site into C*c*P by making a triple mutant (Gly41Glu, Val45Glu, His181Asp, called MnC*c*P) (*30*). The engineered Mn(II)-binding site in C*c*P showed similar spectroscopic properties to those of the corresponding site in MnP as characterized by UV−vis and paramagnetic ^{1}H NMR studies (*30*). More importantly, the engineered enzyme showed more than 5-fold increase in MnP activity compared to WtC*c*P, as measured by its ability to oxidize Mn(II) to Mn(III) (*30*). Similar work has recently been described by Wilcox et al. (*32*), who engineered the Mn(II)-binding site in C*c*P at the location similar to ours (*30*). Despite the different mutations employed in the two designs, the Mn(II)-binding affinity and MnP activity are strikingly similar in the two systems reported (*30*, *32*).

Since designing and creating metal-binding sites in proteins is still a field in its infancy (*29*, *33*), a detailed structural characterization will allow us to understand the impact of creating the Mn(II) site on both the local and global structures of the enzyme. A full structural characterization on the engineered protein MnC*c*P will provide a structural basis for engineering the next generation of C*c*P variants that mimic MnP more closely in both structure and function. To this end, we have carried out detailed paramagnetic NMR characterizations of the resting-state and cyanide-bound forms of MnC*c*P. The location of the Mn(II) site is firmly identified. Our results indicate that the creation of the Mn(II)-binding site in C*c*P caused no detectable structural changes on the distal heme pocket of the protein, but significant structural changes on the proximal side of the heme cavity. More importantly, we found that engineering

the Mn(II) center in C*c*P resulted in a significant weakening of the heme Fe(III)−N(His) bond. Our findings here complement X-ray crystallographic studies well (*10*, *25*, *32*) and provide insights into both geometric and electronic structural changes in *solution*.

EXPERIMENTAL SECTION

Sample Preparation. MnC*c*P was expressed, isolated, and purified according to the methods described previously (*30*). Samples for NMR experiments were concentrated in Centricons (Amicon, Inc.) to final concentrations of 1−2 mM. Protein concentrations were determined using an extinction coefficient of 93 mM^{-1} cm^{-1} at 411 nm (*30*).

Protein samples for NMR experiments were prepared in either D_2O buffer or 90% H_2O/10% D_2O buffer containing 100 mM potassium phosphate at pH 6.0 (uncorrected for any isotope effects). Samples in D_2O were prepared by at least 5 times isotope exchange of the protein solution in H_2O buffer with D_2O buffer at pH 6.0. The isotope exchanges were carried out in either a Centricon or a stirred ultrafiltration cell (both from Amicon, Inc.) at 4 °C. The cyanide adducts of the protein were prepared by addition of a 10−20% molar excess of cyanide from a freshly made 500 mM stock solution of KCN in 99.9% D_2O (Aldrich) to the native enzyme. The pH of the protein solutions was adjusted with dilute DCl or NaOD following the method suggested in the literature (*34*) to avoid local pH extremes for the variable-pH experiment. The pH of the protein solutions is monitored before and after each experiment using a standardized calomel combination microelectrode (Aldrich) attached to an Orion 720A pH meter.

Electronic Absorption Spectroscopy. All electronic absorption spectra were measured at 25 °C with a Hewlett-Packard 8453 diode-array spectrophotometer equipped with a circulating water bath. The pH titration experiments were carried out by dissolving the appropriate amount of protein in 3 mL of 100 mM potassium phosphate, and the pH was adjusted with dilute HCl or NaOH.

NMR Spectroscopy. Proton NMR spectra of both native and cyanide-bound forms of MnC*c*P samples were recorded at 25 °C (except for the variable-temperature experiments) on a Varian Unity 600 FT NMR spectrometer operating at a proton frequency of 599.97 MHz. The ^1H NMR spectra of the ferric native MnC*c*P were collected with a 120 kHz spectral width, 8192 complex data points, and a repetition rate of approximately 40 per second. Typically, 20 000−40 000 scans were collected for each spectrum. Free induction decays were exponentially multiplied by a line-broadening factor of 80−100 Hz before Fourier transformation to improve the signal-to-noise ratio of the spectra.

NMR spectra of the ferric low-spin forms were obtained by collecting 1000−2000 scans with 16 384 complex data points over a 39 kHz bandwidth, and a repetition time of 0.5 s with solvent presaturation during relaxation delay. The spectra were obtained by multiplication of the free induction decays with a 10−20 Hz apodization. Fast repetition spectra of the low-spin protein−cyanide complexes were also recorded with a 120 kHz sweep width, 2048 data points, and a repetition rate of 10 ms to detect the fast-relaxing proton signals which are intrinsically broad. Chemical shift values were referenced to the residual HDO signal at 4.76 ppm.

Variable-temperature experiments were carried out on a Varian Keck 750 spectrometer operating at a proton frequency of 750.12 MHz. The temperature of the probe was controlled by a FTS (Model TC-84) VT system. Chemical shifts were referenced to the residual HDO signal at the appropriate temperature.

The spin−lattice relaxation times of the hyperfine-shifted protons for the cyanide complex of MnC*c*P were measured by the standard inversion−recovery method using the 180°−τ−90°− AQ pulse sequence (*35*). A repetition rate of 1 per second and a 90° transmitter pulse of 9.6 μs were used. The T_1 values were extracted by a nonlinear least-squares fitting routine that employs the equation:

$$M_Z = M_0 (1 - \rho e^{-\tau/T_{1\ obs}}) \quad (1)$$

where τ is the interval between 180° and 90° pulses, M_Z is the *Z*-component of the nuclear magnetization (represented by the intensity of the peak) when the interval is τ, M_0 is the *Z*-component of the nuclear magnetization when the interval is infinite, and ρ is a parameter which becomes 2.0 at the 180° pulse. For signals whose intensities cannot be fitted to eq 1, the T_1 values were estimated from the null point with the relationship of $T_1 = \tau/\ln 2$. The NOE experiments on the cyanide complex of the protein were performed by irradiation of the resonance of interest prior to the 90° pulse. Typically, the peak of interest was irradiated for 100 ms with a weak decoupler power and a repetition time of 0.5 s to obtain steady-state NOEs.

Phase-sensitive NOESY spectra for the cyanide-bound form of MnC*c*P were acquired on the Varian 600 spectrometer at 25 °C with mixing times ranging from 5 to 70 ms. Typical NOESY spectra were collected with 256 experiments in the F1 dimension using the hypercomplex method of States et al. (*36*). In general, 800 scans were accumulated for each F1 experiment, which was acquired with 4096 complex points in the F2 dimension over a spectral width of 39 kHz. The residual intense solvent signal in all NOESY experiments was suppressed using a 200 ms presaturation with a weak decoupler power. NOESY spectra were processed on a Silicon Graphics Indigo 2 Extreme work station using Felix 97 (MSI, Inc.). Data were multiplied with a 60° shifted sine-squared bell window function in both dimensions and were zero-filled to obtain 2K × 2K 2D matrixes as required by the large hyperfine shift dispersion exhibited by the paramagnetic nature of this protein.

Samples for ^{15}N experiments were prepared by addition of 20% excess $NaC^{15}N$ to native MnC*c*P in D_2O buffer. Spectra were collected at 76 MHz in 10 mm sample tubes with deuterium as the frequency lock. The chemical shift for ^{15}N was referenced to NO_3^- as the external standard.

RESULTS

Electronic Absorption Spectroscopy. The electronic absorption spectra of MnC*c*P at various pH are shown in Figure 2. At pH below 6, the protein displays absorptions at 408, 499, 538, and 623 nm, typical of a six-coordinate high-spin (HS) Fe(III) derivative. As the pH is increased, the intensity of the above absorptions decreases, and new absorption bands at 416, 535, and 568 nm appear, indicating that a six-coordinated, low-spin (LS) species is formed, probably due to ligation of an ^-OH ion or another unknown ligand onto

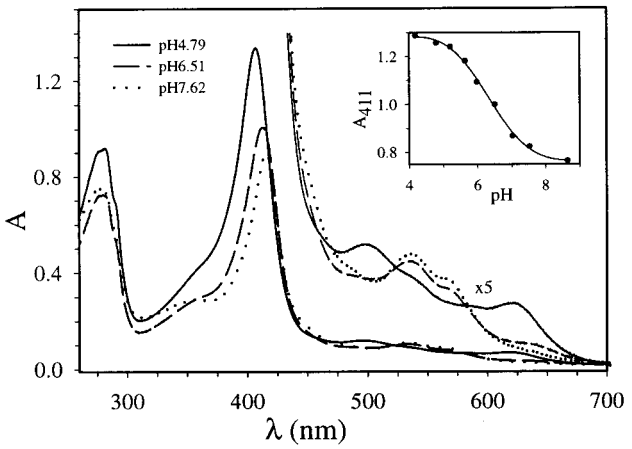

FIGURE 2: UV−vis absorption spectra of MnC*c*P in 0.1 M phosphate (298 K) at different pHs: (—) pH 4.79; (− −) pH 6.51; and (···) pH 7.62. Inset: pH-dependent absorption changes at 411 nm.

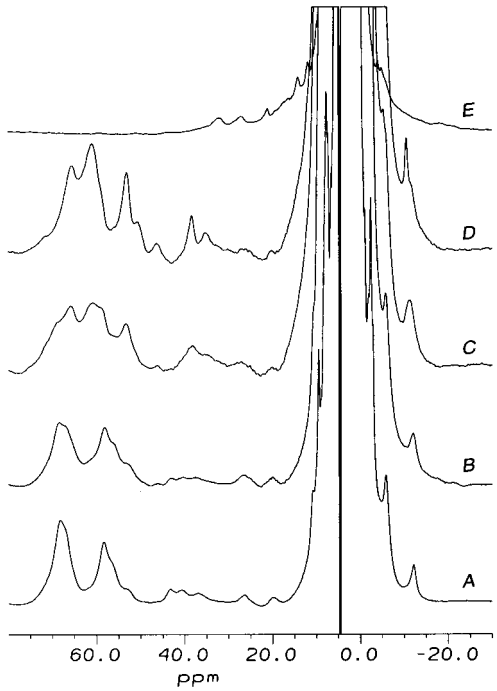

FIGURE 3: 600 MHz ^{1}H NMR spectra of native MnC*c*P (298 K) in 0.1 M phosphate buffer at different pHs. (A) pH 4.79, (B) pH 5.20, (C) pH 5.63, (D) pH 5.97, and (E) pH 7.58.

the heme iron. The pK_a of this ligand is estimated to be 6.5, based on the pH dependence of spectral changes at 411 nm (Figure 2, inset). This pH-dependent spin state change has been observed in several other C*c*P variants (*32*, *37*, *38*). Interestingly, this pH-dependent spin state transition is completely reversible. Further support for this reversible, pH-dependent spin state transition comes from the NMR experiments shown below.

NMR Spectroscopy of Native MnCcP. The 600 MHz ^{1}H NMR spectra of MnC*c*P in 0.1 M potassium phosphate buffer at different pH conditions collected at 25 °C are shown in Figure 3. Comparison of the MnC*c*P spectra collected at pH 6.0 or lower with those reported for WtC*c*P (*37*, *39*) clearly shows similarities in the hyperfine shift pattern between the two proteins. Both WtC*c*P and MnC*c*P display broad resonances and large downfield shifts. The broad resonances and large downfield shifts observed for WtC*c*P have been attributed to the high-spin nature of the protein (*39*−*41*). Therefore, the chemical shift values and the line shapes of MnC*c*P (Figure 3) suggest that this protein is predominantly high spin in the pH range from 4.8 to 6.0. The differences in the chemical shift values may be attributed to the different coordination sphere or geometry at the heme center in the two systems (*37*, *38*). Compared to the spectra of WtC*c*P (*37*, *39*), the spectra of MnC*c*P shown in Figure 3 are about 10 ppm less downfield shifted. Furthermore, the spectrum of MnC*c*P is more comparable with those of the fluoride derivatives of WtC*c*P and the D235N mutant of C*c*P which have been proven to contain a six-coordinate high-pin Fe(III) (*39*, *42*). These observations strongly suggested that the resting state MnC*c*P contains a six-coordinate high-spin Fe(III) and corroborated the conclusion drawn from the electronic absorption spectral study of the protein. The presence of six-coordinate high-spin Fe(III) has been reported for different heme peroxidases (*43*) and other C*c*P variants (*37*, *38*). The sixth ligand to the heme Fe has been inferred to be a water molecule in these proteins (*37*, *38*, *43*).

Careful examination of the spectra shown in Figure 3 reveals that the spectrophotometrically and chromatographically homogeneous MnC*c*P is actually NMR spectroscopically inhomogeneous. This is reflected by the asymmetry of the heme methyl signals and the presence of some minor resonances at 72 and 53 ppm. The presence of multiple forms of MnC*c*P is also supported by a temperature-dependent study on the high-spin form protein (see Supporting Information). The anti-Curie behavior of the hyperfine-shifted signals in MnC*c*P has been observed for WtC*c*P previously and has been attributed to the existence of a solution-state dynamic equilibrium involving a temperature-dependent population of a thermally accessible excited state (*39*). Further evidence for the presence of at least two spectroscopically detectable protein forms comes from the spectra of cyanide-bound low-spin protein that will be discussed in detail later.

When the solution pH is increased from 6.0 to 6.5, the number of resonances attributable to the high-spin form of the protein increases accompanied by a decrease in their intensity (data not shown). A similar result has been reported for the Asp235Ala variant of C*c*P (*37*). This observation was explained as the presence of an equilibrium between the high-spin species and two low-spin species (*37*). One of the low-spin species is in fast equilibrium and the other in slow equilibrium with the high-spin-state species on the NMR time scale. When the pH is increased to 7.6, the low-spin form becomes the principal species of the protein as reflected by the very limited hyperfine-shifted region (within 40 ppm) and the narrower line widths of the shifted resonances (Figure 3E). This is in complete agreement with the spin state transition indicated by electronic spectroscopy over the same pH range

NMR Spectroscopy of MnCcP-Cyanide Complex. Although not physiologically active, the cyanide derivatives of heme peroxidases have been the most favorable systems on which paramagnetic NMR investigations are carried out (*44*−*54*). The short electronic relaxation times and large magnetic anisotropy of the low-spin peroxidase cyanide complexes give much sharper and better resolved signals in their proton NMR spectra, providing much more information about the electronic, magnetic, and molecular structural properties of

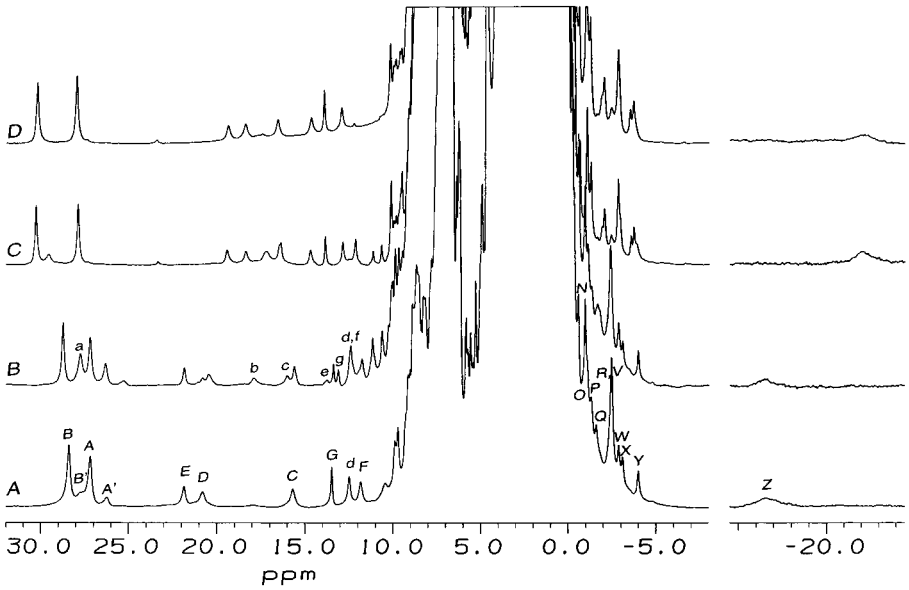

FIGURE 4: 600 MHz ^{1}H NMR spectra of the low-spin cyanide complexes of (A) MnC*c*P in D_2O, (B) MnC*c*P in H_2O, (C) WtC*c*P in H_2O, and (D) WtC*c*P in D_2O. Signals labeled with lower case letters are solvent-exchangeable. Spectra are collected at 298 K in 0.1 M phosphate buffer at pH 6.0.

the heme pocket as compared to the native, high-spin resting forms (*45*, *47*, *54*).

The ^{1}H NMR spectra of the cyanide-bound MnC*c*P complex (MnC*c*PCN) in 0.1 M potassium phosphate buffer are shown in Figure 4A (in D_2O) and Figure 4B (in H_2O). The spectral features of MnC*c*PCN display a high degree of similarity to that of WtC*c*PCN shown in Figure 4C,D. In D_2O solution (Figure 4A), the downfield spectral regions (approximately 10−32 ppm) of MnC*c*PCN and WtC*c*PCN (Figure 4C) show exactly identical numbers of resonances at fairly comparable positions. The two intense signals with integrated intensities of three protons each in the downfield region are typical of heme methyl groups. Other resonances with intensities of one proton each in the downfield region represent protons from other heme substituents and those from amino acid residues in the proximal and distal heme pocket. The resolved upfield spectral region displays several single-proton resonances, two multi-proton signals, and an extremely broad signal at approximately −16.5 ppm. Previous work on both heme model compounds and a number of heme peroxidases has firmly concluded that this spectral region encompasses the resonances from β-protons of the heme vinyl and propionate groups as well as those from some of the amino acid residues near the heme center (*54*−*56*). Additional peaks were detected when the spectrum was recorded in H_2O solution (Figure 4B). These solvent-exchangeable resonances provide valuable information for the unambiguous assignment of the hyperfine-shifted signals of MnC*c*P as was in the case of WtC*c*P (*44*, *57*). The chemical shifts and spin−lattice relaxation times for the hyperfine-shifted resonances and their assignments in MnC*c*PCN are compiled in Table 1, along with the corresponding parameters in WtC*c*PCN (*44*, *57*) and MnPCN reported previously (*58*, *59*).

Comprehensive inspection of the 1D NMR spectra of MnC*c*PCN collected in D_2O (Figure 4A) and H_2O (Figure 4B) reveals that in addition to the presence of additional signals in H_2O, there is a small solvent isotope effect on the shifts of some heme resonances. This isotope effect was also observed in other peroxidase systems, such as HRPCN (*60*) and MnPCN (*58*), and had been attributed to the partial deuteron/proton interchange on a group that interacts with protons displaying such isotope shifts (*58*, *60*). The labile proton/deuteron responsible for the observed solvent isotope effect on heme resonances has been shown to reside on the Nϵ atom of the distal histidine (*60*).

It is interesting to note that the NMR spectra of MnC*c*PCN in both D_2O and H_2O buffers (Figure 4A,B) display resonances that are indicative of at least two protein forms in solution under the conditions employed in this study. Further evidence for the presence of multiple forms of MnC*c*P comes from the temperature-dependent experiment shown in Figure 5. The fact that the exact concentration of each form is dependent on the temperature indicates that the major and minor forms of this protein are in equilibrium with each other.

Assignment of the Hyperfine-Shifted NMR Signals for the MnCcPCN Complex. The assignment of the hyperfine-shifted signals for the MnC*c*PCN complex was achieved through comparison with the assignments made for WtC*c*PCN and MnPCN (Table 1) (*42*, *44*, *49*, *50*, *57*, *58*, *61*) and examination of the active site structure of WtC*c*P revealed by its crystal structure with confirmation through 1- and 2-dimensional NOE measurements as well as through-bond connectivities (COSY). Some typical 1D NOE difference spectra are shown in Figure 6B−6G. Figure 7A shows the NOESY spectra of MnC*c*PCN collected in D_2O buffer with a mixing time of 35 ms. The clear NOESY connectivities in Figure 7 and the results from through-bond (COSY) connectivities (see Supporting Information) prove the validity of NOE connectivities observed in 1D NOE experiments (Figure 6) and lead to the unambiguous assignments for all of the nonexchangeable hyperfine-shifted protons from the heme active site in MnC*c*PCN. The assignment for the solvent-exchangeable resonances was achieved through NOESY experiments carried out in 90% H_2O/10% D_2O buffer (see Supporting Information). The assignment of the protons close to the designed Mn(II)-binding site was further

Table 1: Proton NMR Parameters and Assignments of Paramagnetically Shifted Resonances in MnC*c*PCN at 289 K, in 0.1 M Phosphate Buffer, pH 6.0. Parameters for WtC*c*PCN and MnPCN Are Included for Comparison[a]

	MnCcPCN		WtCcPCN[b]		MnPCN[c]		
signal	δ (ppm)	T_1 (ms)	δ (ppm)	T_1 (ms)	δ (ppm)	T_1 (ms)	assignment
							heme
B	28.4	43	27.6	39	20.4	92	8-CH_3
A	27.2	65	30.6	40	30.7	67	3-CH_3
E	21.9	101	16.0	60	12.7	*d*	4-Hα
D	20.8	87	18.3	45	12.5	70	7-Hα
	8.30[e]	*f*	6.4	*d*	8.0	*d*	7-Hα'
	7.05[e]	*f*	5.31[g]	*d*	7.0	*d*	δ-meso
	6.79[e]	*f*	7.1	*d*	8.6	*d*	2-Hα
	4.33[e]	*f*	5.84[g]	*d*	*d*	*d*	β-meso
	3.62[e]	*f*	*d*	*d*	−1.1	*d*	α-meso
	3.24[e]	*f*	*d*	*d*	*d*	*d*	6-Hα[h]
	1.98[e]	*f*	3.0	*d*	*d*	*d*	7-Hβ
	1.84[e]	*f*	*d*	*d*	*d*	*d*	6-Hα[h]
M	−0.19	*f*	−1.3	*d*	*d*	*d*	7-Hβ'
	−1.24[e]	*f*	*d*	*d*	*d*	*d*	γ-meso
P	−1.29	*f*	*d*	*d*	*d*	*d*	6-Hβ[h]
Q	−1.58	*f*	*d*	*d*	*d*	*d*	6-Hβ[h]
V	−2.44	*f*	−3.0	*d*	−3.2	*d*	2-Hβ_{trans}
W	−2.85	*f*	−2.1	*d*	−1.8	140	4-Hβ_{trans}
X	−3.08	*f*	−3.7	*d*	−3.4	*d*	2-Hβ_{cis}
Y	−3.98	*f*	−3.8	*d*	−2.8	165	4-Hβ_{cis}
							Arg48
b	17.8	*i*	17.8	13	*j*	*j*	NH[k]
e	13.8	*i*	*d*	*d*	*j*	*j*	NH[k]
g	13.1	*i*	*d*	*d*	*j*	*j*	NϵH
f	12.3	*i*	12.3	200	*j*	*j*	NH[k]
	11.2	*i*	*d*	*d*	*j*	*j*	NH[k]
	6.47	*f*	7.18[l]	*d*	*j*	*j*	CαH
O	−1.08	*f*	−1.52[g]	*d*	*j*	*j*	CδH
R	−2.36	*f*	−3.28[g]	*d*	*j*	*j*	CβH
							His52
a	27.7	*i*	28.4	7	34.2	15	Hϵ2
c	16.0	*i*	16.5	*d*	17.0[m]	*d*	Hδ1
G	13.5	216	14.0	67	12.8[m]	*d*	Hϵ1
							Ala174
	9.74[e]	*f*	10.0[g]	*d*	*d*	*d*	NpH
	2.18[e]	*f*	2.65[g]	*d*	*d*	*d*	Hα
M	−0.19	*f*	0.30[g]	*d*	*d*	*d*	CβH
							His175
C	15.7	68	19.4	34	19.5	53	Hβ
d	12.5	130	12.9	110	12.4	*d*	NpH
F	11.8	94	14.8	34	16.9	86	Hβ'
	8.79[e]	*f*	10.2	*d*	15.1	29	Hδ1
	5.76[e]	*f*	8.48[g]	*d*	*d*	*d*	Hα
	−16.5	< 5	−20.6	2.5	−11.8	2.5	Hϵ1
							Ala176
	8.47[e]	*f*	6.99[g]	*d*	*d*	*d*	NpH
							Thr180
	4.06[e]	*f*	*d*	*d*	*d*	*d*	CαH
	3.36[e]	*f*	2.80[j]	*d*	*d*	*d*	CγH
							Leu232
	0.48[e]	*f*	0.7	*d*	*d*	*d*	CγH
	−0.93	*f*	−1.1	*d*	*d*	*d*	δ-CH_3
V	−2.44	*f*	−2.6	*d*	*d*	*d*	δ-CH_3'

[a] Lower case letter labeling indicates exchangeable protons. [b] Taken from (*44*). [c] Taken from (*58*). [d] Not reported in the reference cited. [e] The shift value was measured from the 2D map collected at 600 MHz. [f] Not measured because the signal is in the complex envelope. [g] Taken from (*57*). [h] Specific methylene assignments not confirmed. [i] No effort was made to determine the T_1 values for exchangeable protons. [j] The corresponding signal is not observed in MnPCN. [k] Assignment to specific nitrogen proton not confirmed. [l] Taken from (*61*). [m] Taken from (*59*).

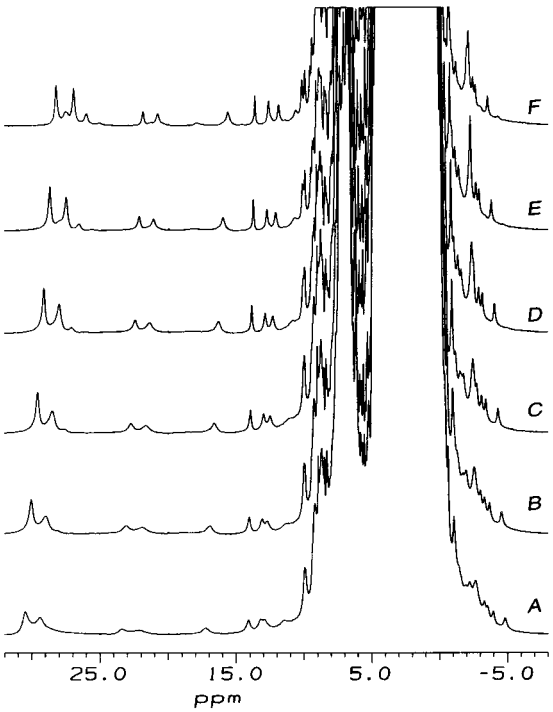

FIGURE 5: 750 MHz ^{1}H NMR spectra of 1.6 mM MnC*c*PCN in D_2O, 0.1 M phosphate buffer, pH 6.0, at different temperatures. (A) 278 K, (B) 283 K, (C) 288 K, (D) 293 K, (E) 298 K, and (F) 303K.

confirmed with addition of 0.4 equiv of Mn^{2+} which resulted in specific broadening of paramagnetically shifted signals "D", "M", "P", and "Q" and their corresponding cross-peaks as shown in Figure 7B.

(a) The Heme Substituents. As shown in Figure 6B, irradiation of the heme methyl resonance "B" yields detection of weak NOEs to peak "D" at 20.8 ppm and a peak at 8.3 ppm in the difference spectrum. Several other peaks are also observed in the difference spectrum in the diamagnetic aliphatic region, attributable to amino acid residues close to the methyl group being saturated. Reciprocal NOE to signal "B" is observed when resonance "D" is saturated as shown in Figure 6C. Peak "D" also displays primary NOEs to signals at 8.30, 4.06, 3.36, 1.98, and −0.19 ppm. These NOE connectivities are quite comparable with those observed for WtC*c*PCN and HRPCN, which leads to the assignment of resonance "B" to the 5- or 8-CH_3 group (*44*, *50*, *51*, *58*, *62*).

Irradiation of the other heme methyl signal "A" at 27.2 ppm produces an extremely weak NOE to resonance "E" at 21.9 ppm and weak NOE signals at 6.79, −2.85 (resonance "W"), and −3.98 ppm (resonance "Y", Figure 6D). Saturation of signal "E" yields NOEs to resonances "W", "Y", and reciprocal NOE to signal "A" (Figure 6E). No detectable NOE is observed between resonance "E" and the signal at 6.79 ppm, excluding the geminal partner relationship between these two resonances which would otherwise produce strong NOE connectivity. Therefore, resonance "E" must be assigned to the αH of a vinyl group and signal "A" to a nearby methyl group. Consequently, signals "W" and "Y" must be assigned to the β-protons of the same vinyl group. This is consistent with the expected chemical shift pattern of a vinyl group. The α-CH vinyl proton resonance is normally observed in the downfield region because of π-spin delo-

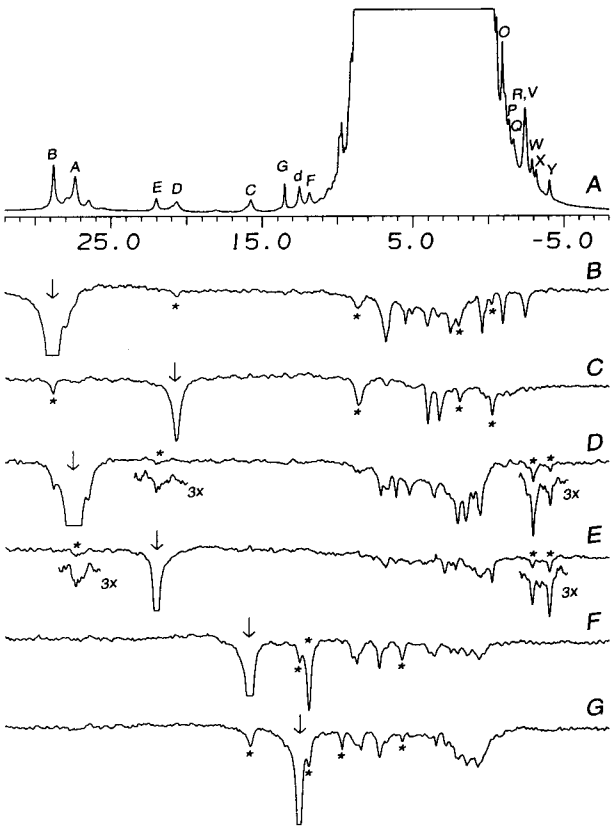

FIGURE 6: 600 MHz ^{1}H NMR spectra of 1.6 mM MnC*c*PCN in D_2O, 0.1 M phosphate buffer, pH 6.0, at 298 K. (A) Absorption spectrum; (B−G) NOE difference spectra obtained upon irradiation of peaks B, D, A, E, C, and d, respectively. The irradiated peak is indicated with a downward arrow in each difference spectrum. Inserts in each spectrum are vertical scale multiplied 3 times.

calization of the unpaired spin density in the vinyl group, whereas the β-CH_2 vinyl proton peaks are usually positioned between 0 and −5.0 ppm (*63*).

The detection of only two of the four heme methyl proton signals outside the diamagnetic region is consistent with earlier observations for WtC*c*PCN and other low-spin hemoprotein cyanide complexes (*51, 62, 64*). The result has been attributed to the particular orientation of the proximal histidine ligand nodal plane with respect to the heme plane (*64*−*67*). Depending on the position of the proximal histidine, the four heme methyls display a unique isotropic shift pattern as either the 1-CH_3 and 5-CH_3 or the 3-CH_3 and 8-CH_3 pair in the downfield region (*64*). The observed resonance "A" for MnC*c*PCN is assigned to the 3-CH_3 group, as irradiation of peak "A" also gives detectable NOE connectivity to a signal at 6.79 ppm. The latter signal is assignable to the αH of the vinyl group other than the vinyl group mentioned before (also see NOESY results below and COSY in Supporting Information). The presence of dipolar connectivities to two vinyl groups mandatorily assigns signal "A" to 3-CH_3, as it is the only candidate that can display such dipolar connectivities. The observed NOE intensity difference between the αH (resonance "E") and βH's of the vinyl group (resonance "W" and "Y") in their respective NOE connectivity with 3-CH_3 (resonance "A") indicates that the αH of the vinyl group is pointing away from the 3-CH_3 group, and the βH of the vinyl group is pointing toward this methyl group as shown in Figure 1A. This is in complete agreement with the results observed for WtC*c*PCN and MnPCN (*50, 58*). This result is also in good agreement with the results obtained from crystallographic analysis of the C*c*P structure (*6, 68*). The position of the 2-vinyl group shown in Figure 1B would produce observable NOE connectivity between the βH (usually in the upfield region) and the 3-CH_3 group as was in the case of LiPCN and HRPCN (*51, 62, 69*). With resonance "A" assigned, signals at 21.9 ("E"), −2.85 ("W"), and −3.98 ("Y") ppm observed in the NOE difference spectrum by saturating peak "A" can be assigned to 4-Hα, 4-H_β-t, and 4-H_β-c, respectively, according to the magnitude of NOEs observed and the scalar connectivities observed in COSY experiment (see Supporting Information). Consequently, peak "B" at 28.4 ppm must originate from the 8-CH_3, and the NOE observed at 20.8 ppm upon saturation of peak "B" must arise from the 7-propionate Hα. Assignment of signal B as the 8-CH_3 group is further supported by the small solvent isotope effect on the shift of this resonance (*58, 60*). Irradiation of signal "D" produces the expected reciprocal NOE to the assigned 8-CH_3 as well as strong NOEs to signals at 8.30, 4.06, 3.36, 1.98, and −0.19 ppm (Figure 6C). The assignment of these signals (Table 1) was achieved by analysis of the relative NOE intensities with signal "D", their relative line widths and shift positions, with confirmation from the connectivities observed in NOESY (Figure 7) experiments. Signals at 4.06 and 3.36 ppm, which display much larger NOEs to signal "D", were assigned to the 7α proton's nearest neighbor threonine 180 (Table 1) based on the analogous assignment made for WtC*c*PCN (*50*).

The above assignments illustrate the close similarity in chemical shifts for corresponding heme resonances between MnC*c*PCN and other peroxidase cyanide complexes, such as WtC*c*PCN, MnPCN, and HRPCN. Therefore, we searched carefully for the 6-propionate resonances of MnC*c*PCN as this is directly related to this protein's ability to bind and oxidize Mn(II). The corresponding resonances in WtC*c*PCN and MnPCN were not resolved since they all fall in the congested diamagnetic envelope of the spectrum (*39, 44, 50, 57, 58, 61*). However, the 6-propionate resonances have been successfully assigned in HRPCN (*46, 62*). Comparison of the ^{1}H NMR spectra of MnC*c*PCN (Figure 4A and Figure 7) and HRPCN (*46, 62*) reveals the most probable candidates (signals Q and P) for 6-propionate resonances in MnC*c*PCN. In HRPCN, the 6-propionate β-protons were observed as an essentially degenerate pair resonating at −2.3 ppm. The similar shift position of signals Q and P in MnC*c*PCN as compared with that of the corresponding signal in HRPCN along with their small shift difference suggested the assignment of resonances Q and P to the β-protons of the 6-propionate group in MnC*c*PCN. Both Q and P yield cross-peaks to a signal at 1.84 ppm and a signal at 3.24 ppm that are assignable to the two α-protons of the same propionate group. The expected NOE between signal P (at −1.29 ppm) and one of the methylene protons from Arg48 (see Table 1) in the distal heme pocket was indeed observed in our NOESY experiment. This suggested that in MnC*c*PCN Arg48 is situated over the same pyrrole as was in the case of WtC*c*PCN (*6*) and HRPCN (*46*).

(b) The Proximal Histidine. The presence of the extremely broad, fast relaxing, far upfield-shifted peak "*Z*" at −16.5 ppm is a characteristic feature of the existence of the proximal histidine within the heme crevice. This peak has

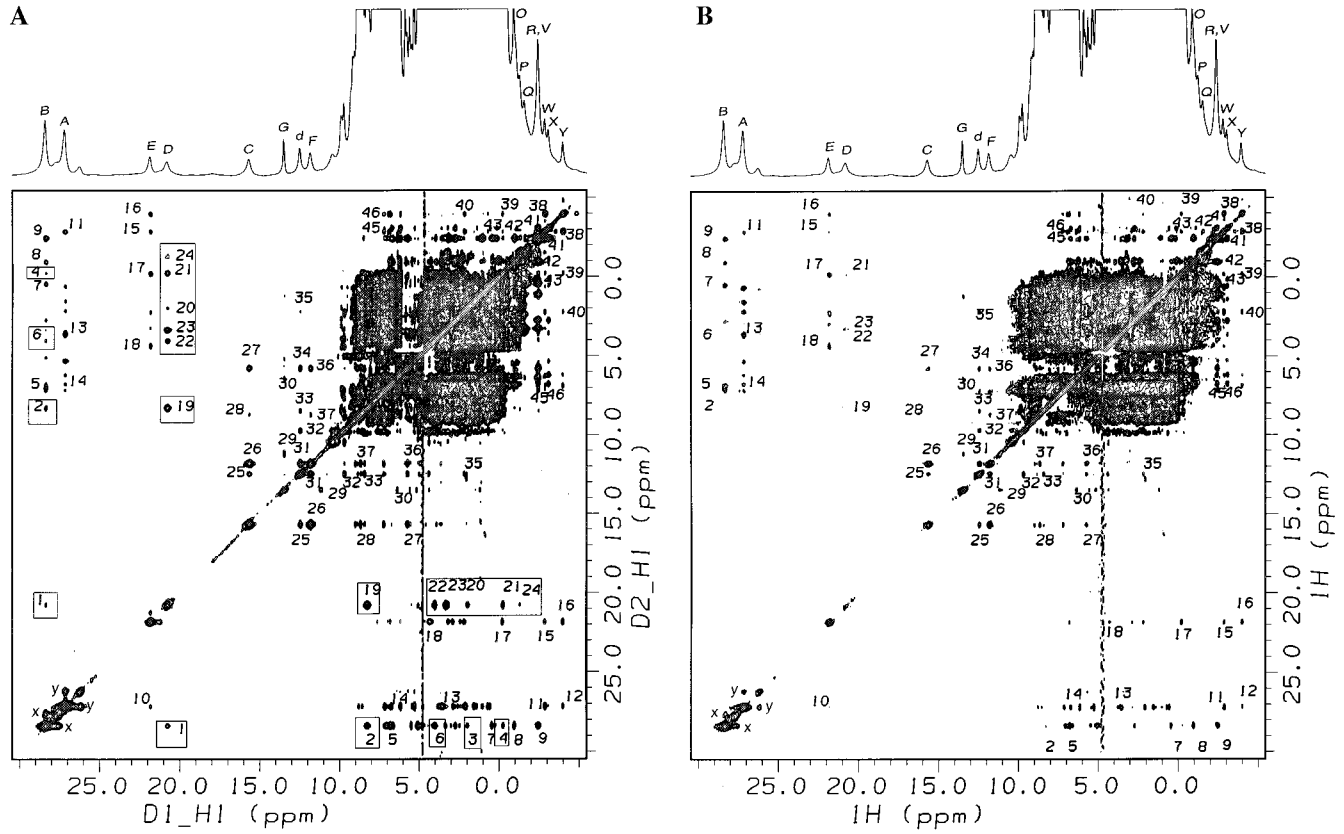

FIGURE 7: 600 MHz phase-sensitive ^{1}H NOESY spectra of 1.6 mM MnC*c*PCN as affected by addition of Mn^{2+}: (A) without Mn^{2+}; (B) with 0.4 equiv of $MnSO_4$. Both spectra are collected with a mixing time of 35 ms. Cross-peaks that either disappear or decrease dramatically in intensity with addition of Mn^{2+} are marked by rectangles in (A). Other conditions are identical to those in Figure 5. Cross-peak assignments: (1) 8-CH_3:7-Hα; (2) 8-CH_3:7-Hα'; (3) 8-CH_3:7-Hβ; (4) 8-CH_3:7-Hβ'; (5) 8-CH_3:H-δmeso; (6) 8-CH_3:Hα Thr180; (7) 8-CH_3:Hγ Leu232; (8) 8-CH_3:δ-CH_3 Leu232; (9) 8-CH_3:δ'-CH_3 Leu232; (10) 3-CH_3:4-Hα; (11) 3-CH_3:4-Hβtrans; (12) 3-CH_3:4-Hβcis; (13) 3-CH_3:Hαmeso; (14) 3-CH_3:2-Hα; (15) 4-Hα:4Hβtrans; (16) 4-Hα:4-Hβcis; (17) 4-Hα:Hβ Ala174; (18) 4-Hα:Hβmeso; (19) 7-Hα:7-Hα'; (20) 7-Hα:7-Hβ; (21) 7-Hα:7-Hβ'; (22) 7-Hα:Hα Thr180; (23) 7-Hα:Hγ Thr180; (24) 7-Hα:Hγmeso; (25) Hβ His175:NHp His175; (26) Hβ His175:Hβ' His175; (27) Hβ His175:Hα His175; (28) Hβ His175:Hδ1 His175; (29) Hϵ1 His52:NH Arg48; (30) Hϵ1 His52:Hα Arg48; (31) NHp His175:Hβ' His175; (32) NHp His175:NHp Ala174; (33) NHp His175:NHp Ala176; (34) NHp His175:Hα His175; (35) NHp His175:Hα Ala174; (36) Hβ' His175:Hα His175; (37) Hβ' His175:Hδ1 His175; (38) 4-Hβcis:4-Hβtrans; (39) 4-Hβcis:Hβ Ala174; (40) 4-Hβcis:Hα Ala174; (41) 2-Hβcis:2-Hβtrans; (42) δ-CH_3 Leu232:δ'-CH_3 Leu232; (43) δ-CH_3 Leu232:Hγ Leu232; (44) δ'-CH_3 Leu232:Hγ Leu232; (45) 2-Hα:2-Hβtrans; (46) 2-Hα:2-Hβcis. Cross-peaks between heme 6-propionate protons and Arg48 protons can only be observed when the NOESY map is expanded.

been previously detected for the low-spin cyanide adducts of a number of heme peroxidases and is assigned to the Hϵ1 of the proximal histidine imidazole ring (*44, 57, 58, 69*−*71*). The line width and chemical shift values of peak "*Z*" in MnC*c*PCN match quite closely to those of the corresponding peak in other cyanide adducts of heme peroxidases. The existence of a proximal His ligand is further supported by the NOE studies shown in Figure 6F,G and the NOE connectivities observed in NOESY experiments shown in Figure 7.

The NOESY spectrum collected with a mixing time of 35 ms (Figure 7) reveals that the peptide NH also displays relatively strong NOE connectivities to resonances at 9.74, 8.47, and 2.18 ppm. Examination of the crystal structure and the relative distances of specific protons from the heme iron combined with the application of sequence-specific assignment methods (*72, 73*) lead to the most probable assignment of these resonances as listed in Table 1. Observation of these NOE connectivities in D_2O buffer suggests that the proximal side of the heme in MnC*c*PCN is essentially inaccessible to the solvent as in the case of WtC*c*PCN (*57*).

(c) The Distal Histidine. The only downfield hyperfine-shifted resonance in D_2O buffer that remains unassigned by now is signal "G" as it displays no NOE connectivity to any other hyperfine-shifted resonances (data not shown). This situation adds uncertainties in assigning this signal. However, the extremely long nonselective T_1 of this signal as compared to other hyperfine-shifted resonances as well as the assignment made for similar resonances in WtC*c*PCN (*44, 57*) and HRPCN (*51, 60, 72*) leads to the assignment of signal "G" to the Hϵ1 of the distal histidine, His52. Further support for this assignment comes from NOESY experiment performed in H_2O buffer (see Supporting Information), where a cross-peak is observed between signal "G" and a labile proton signal, "c", at 16.0 ppm. The latter signal is comparable to the position of 16.5 ppm in WtC*c*PCN and 16.3 ppm in HRPCN, which have been earlier assigned to Hδ1 of the distal His (*44, 57*). Therefore, by analogy with WtC*c*PCN and HRPCN, the resonance at 16.0 ppm observed for MnC*c*P can be assigned to the Hδ1 of His52. Observation of the His52 NδH resonance implies that the distal histidine in MnC*c*P is protonated as it was in the case of WtC*c*PCN and HRPCN (*44, 57*).

(d) Assignment of Arg48. Assignment for Arg48 was achieved primarily by analysis of the NOESY spectra collected in 90% H_2O solution (see Supporting Information).

Resonance "e" displays an NOESY cross-peak with signal "c", while resonance "g" shows dipolar connectivity to peak "G". These NOESY connectivities indicate that resonances "e" and "g" must belong to protons that are positioned in the distal heme cavity and are close to the CϵH and the NδH of the distal histidine. Examination of the crystal structure of WtC*c*P shows that only the NHs of Arg48 are close to Hϵ1 and the Hδ1 of the distal histidine. Therefore, resonance "e" can be assigned to one of the Hη protons and signal "g" to the Hϵ proton of Arg48. With signal "g" assigned, some of the methylene protons of Arg48 can be assigned (Table 1) from the NOESY experiments and the interproton distances measured from the crystal structure of WtC*c*P (*6*).

The last unassigned resonance, "b", displays an exact observed hyperfine shift of 17.8 ppm as the comparable resonance in WtC*c*PCN (*44, 57*). However, the assignment for this exchangeable resonance has been controversial in the literature. We assign this signal to one of the NHs of Arg48 based on the fact that it shows strong NOE connectivity to resonance "d" at 12.4(5) ppm. This assignment can be justified after careful analysis of the line shape of resonance "d" and comparison to the corresponding signal in WtC*c*PCN and HRPCN. In both WtC*c*PCN and HRPCN, signal "d" has been confirmed to be a composite signal with a broader shoulder "f" (*44*) and has been assigned to one of the NHs of Arg48. Signal "d" in MnC*c*PCN clearly shows a broader shoulder at 12.4 ppm. Therefore, resonance "f" can be assigned to an NH of Arg48 on the basis of its comparable hyperfine shift with WtC*c*PCN and HRPCN. Consequently, resonance "b" should be assigned to an NH of Arg48. Thus, the cross-peak is actually between resonances "b" and "f" instead of between signals "b" and "d". Signal "d" has been confirmed to belong to the NpH of His175 and is not expected to show any dipolar connectivity to protons of Arg48.

(e) Leu232 Assignment. The NOESY spectrum shown in Figure 7 clearly shows dipolar connectivities between the firmly assigned heme 8-CH_3 protons and two upfield resonances at -0.93 and -2.44 ppm. In the crystal structure of WtC*c*P, the average distance between heme 8-CH_3 protons and the two δ-methyl protons of Leu232 is within 4 Å, close enough for proton NOEs to be detected between them. Therefore, resonances at -0.93 and -2.44 ppm can be assigned to the two δ-methyl protons of Leu232. This assignment is further supported by the comparative integration of at least three protons for each of these two resonances relative to the firmly assigned heme 8- and 3-CH_3 resonances. Assignment of Leu232 to the upfield resonances has been reported for WtC*c*PCN (*44, 57*).

^{15}N NMR Measurements. To further investigate the heme active site coordination environment of the MnC*c*PCN complex, ^{15}N NMR experiments were carried out. The ^{15}N NMR spectrum of MnC*c*PCN shows a broad signal at 612 ppm (data not shown). This ^{15}N NMR shift falls in the corresponding ^{15}N shift region for several other peroxidases reported previously, with 587, 608, and 639 ppm observed for WtC*c*PCN, LiPCN, and MnPCN, respectively (*15, 37, 59, 74*−*77*). It has been reported that this ^{15}N NMR shift is directly related to the strength of the axial ligand−iron bond (*15, 74*−*78*).

DISCUSSION

pH-Dependent Spin State Changes and Presence of Multiple Forms of MnCcP. Unlike WtC*c*P which contains a predominantly five-coordinated ferric iron center at high-spin state over a wide range of pH (*79*), the engineered protein MnC*c*P exhibits two spectrophotometrically distinct species that are interconvertible between pH 4.8 and 7.6 (Figure 2). Below pH 6.0, the protein displays an electronic absorption spectrum typical of hexacoordinated, high-spin ferric hemoproteins. This is reflected by the clear shoulder (the δ band) near 380 nm, a charge-transfer band (CT) $>$620 nm, and a relatively large A_{Soret}/A_{380} (2.42) ratio. The corresponding ratio in the high-spin, pentacoordinated WtC*c*P (1.51) is smaller than that observed here (*79*). The presence of a hexacoordinated high-spin heme iron in MnC*c*P below pH 6.0 is further supported by the similar, but 10 ppm less downfield shift of the ^{1}H NMR spectra of MnC*c*P compared with that of WtC*c*P, and by the close similarity of MnC*c*P to the fluoride derivatives of WtC*c*P and the D235N mutant, which have been proven to contain a six-coordinate high-spin Fe(III). Similar observations have been reported for other C*c*P variants, and the sixth ligand to the heme iron has been suggested to be a water molecule (*37, 38*).

When the solution pH is increased above 6.5, the electronic absorption spectrum of MnC*c*P clearly changes to that of a hexacoordinated, low-spin state (Figure 2E), in agreement with results obtained on other C*c*P mutants reported in the literature (*37, 38, 80*). The engineered C*c*Ps containing Mn(II)-binding sites carried out by Wilcox et al. (*32*) also display low-spin heme UV−vis spectra at 100 mM phosphate, pH 6.0. Further evidence of the presence of a low-spin-state heme iron comes from the ^{1}H NMR spectra of this protein collected at pH above 6.5 (Figure 3E). Previous studies have established the identity of the sixth ligand to be either a hydroxide ion or the side chain of the distal histidine (*37, 38, 80*). Both electronic and ^{1}H NMR spectra of MnC*c*P at pH above 6.5 are similar to those reported for the Asp235Ala mutant of C*c*P (*37*) between pH 6.0 and 6.7 and those observed for hydroxide-bound metmyoglobin (*81, 82*). Therefore, it is suggested that at pH above 6.5, the sixth ligand of the heme iron in MnC*c*P is a hydroxide ion which derives from the deprotonation of the heme-bound water molecule at low pH. Compared to other hydroxide complexes of ferriheme proteins, such as metmyoglobin, the pK_a (the pH at which the spin state change occurs) of the bound water molecule in MnC*c*P is more than 1 pH unit lower (*83*). This dramatically lowered pK_a of the heme iron bound water in peroxidases has been attributed to the presence of a positively charged residue (Arg48 in C*c*P) and other polar residues in the distal heme pocket as compared to those present in globins (*37*). It has also been suggested that the properties of the heme-bound water molecule are affected by the strength of the proximal heme ligand with stronger proximal ligand favoring the H_2O form and weaker proximal ligand preferring the $^-$OH form.

The NMR spectra of MnC*c*PCN in both D_2O (Figure 4A) and H_2O (Figure 4B) buffers display asymmetric heme methyl resonances and some minor resonances in addition to the major resonances. These small peaks (peaks A′ and B′, for example) were initially thought to be from the impurities escaped from the purification procedure. However,

results from NOESY experiments (Figure 7) definitely argue for a different form of the protein giving rise to these small peaks. The NOESY spectrum collected with mixing times as short as 5 ms clearly reveals intense cross-peaks (labeled x and y) connecting the corresponding peaks A−A′ and B−B′ (see Supporting Information). The strong cross-peaks x and y in the NOESY spectra can be explained as exchange peaks attributable to an exchange process in which the heme methyl groups sample two inequivalent magnetic environments. This explanation is further supported by saturation transfer experiments where a significant intensity loss of signal A is observed when signal A′ is irradiated (data not shown). An identical result is obtained when the inverse irradiation experiment is performed. Comparable results are observed when saturation transfer experiments are performed on signals B and B′. A similar phenomenon has been observed previously and has been interpreted as the presence of a minor form (or forms) of the protein which represents different conformations of the parent enzyme (*84, 85*). The exact source of this heterogeneity has not been clarified, but the presence of the minor form does not compromise the experiments and conclusions drawn for the predominant component protein in this study.

Further evidence for the presence of an equilibrium between multiple forms of MnC*c*P comes from a temperature-dependent experiment (Figure 5). When the spectrum is collected at 5 °C, only one form is predominant since the presence of the minor signals is hardly detectable. When the temperature is raised, the fraction of the minor form enzyme increases as reflected by the intensity increase of the peaks from the minor enzyme form. When the spectrum is collected at 30 °C, the highest temperature employed in this study, the fraction of the minor form enzyme increased to about 25% of the total protein present in solution. Although no spectra were taken at temperatures higher than 30 °C as restricted by the stability of the sample, we predict that higher temperatures would invert the predominance of the two protein forms. It should be pointed out that the combined relative intensities of each pair of signals A/A′ and B/B′ remained constant throughout the temperature range employed, suggesting the existence of an equilibrium between two forms which complies with the conclusion drawn from NOESY experiments.

It is interesting to note that not all of the hyperfine-shifted resonances display corresponding partners in the NMR spectra. In fact, only two signals show a doubled-peak pattern and display pairwise intensity ratio changes as shown in Figure 5. This fact combined with the very similar chemical shifts of the two protein forms suggests that there is no global conformational differences between the two distinguishable protein forms. It seems that the magnetic inequivalence is particularly localized to a specific region of the heme active site.

Location of Mn(II)-Binding Sites. The successful assignments of paramagnetically shifted signals make it possible to locate the engineered Mn(II)-binding site in MnC*c*P. Since the unpaired electrons of Mn(II) can interact with protons close to Mn(II) and broaden them, observation of broadening of specific signals indicates specific Mn(II) binding and helps locate the Mn(II)-binding site. As shown in Figure 7B, upon addition of 0.4 equiv of Mn^{2+}, signals "D", "M", "P", and "Q" and their NOE cross-peaks (highlighted in boxes in Figure 7A) either disappear completely or decrease dramatically in their intensity. Those signals have been assigned to be the protons of the propionate groups, which are around the putative Mn(II)-binding site.

Overall and Local Structural Changes Associated with the Introduction of the Mn(II) Site. From comparison of the resonance assignments made for HRPCN and WtC*c*PCN with the assignments made for MnC*c*PCN presented above, it is clear that the three enzymes display remarkable similarities in their ^{1}H NMR spectra. In all three enzymes, the proximal and distal histidine protons as well as the heme 8-CH_3, 3-CH_3, 4α-protons, and 7α-protons resonate downfield. The heme vinyl and propionate β-protons all fall in the upfield region of the spectra. In particular, the hyperfine shifts displayed by the distal histidine protons are almost identical within the three protein systems. Since the distal histidine in cyanide derivatives of heme peroxidases never binds directly to the heme iron, the hyperfine shifts exhibited by protons in this residue are primarily attributed to the pseudocontact effect. Since pseudocontact shifts are determined by the magnetic susceptibility tensor, it is thus concluded that the magnetic axes are oriented similarly in all three enzyme systems, as was described previously for HRPCN (*48, 51, 57, 60, 62*). The hyperfine shifts of the peptide NH of the proximal histidine in all three enzyme systems are also nearly identical (Table 1), further suggesting a similar orientation of the magnetic susceptibility tensor within these three protein systems. The peptide NH of the proximal histidine is more than four bonds away from the heme iron; thus, its hyperfine shift is expected to be primarily due to the pseudocontact effect.

While construction of a Mn(II)-binding site in C*c*P introduces non-detectable structural change in the distal heme crevice as evidenced by the relatively insensitive shifts displayed by the distal residues, noticeable structural rearrangements for the proximal histidine are observed as reflected by the dramatic changes in the chemical shift displayed by the protons of this residue. Of particular interest, the chemical shift of CϵH of the proximal histidine ligand has been shown to correlate with the heme Fe(III)−N(His) bond strength in a number of heme proteins (*69*). The shift of CϵH of the proximal histidine in MnC*c*PCN strongly indicates a weaker heme Fe(III)−N(His) bond compared to that in WtC*c*PCN. This is in good agreement with the result from the ^{15}N NMR experiment on MnC*c*PCN (vide infra). Interestingly, the hyperfine shift pattern of the proximal histidine protons in MnC*c*PCN more closely resembles that observed in MnPCN than in WtC*c*PCN (Table 1). The peptide NH protons of the proximal His in the two enzymes resonate at an essentially identical position (12.4 ppm). The separations in shift for the β-CH_2 protons are also comparable (3.9 ppm in MnCcPCN, 2.6 ppm in MnPCN) between the two enzymes.

^{15}N NMR Chemical Shifts and Heme Fe(III)−N(His) Bond Strength. The ^{15}N NMR chemical shift of the bound cyanide anion in hemoproteins is a highly sensitive indication of the donor strength of the proximal histidyl ligand. Proteins with a stronger heme Fe(III)−N(His) bond have ^{15}N shift values in the relatively upfield region (HRP 576 ppm, WtC*c*P 587 ppm), while proteins with a weaker heme Fe(III)−N(His) bond display relatively downfield shift of this signal (LiP 608 ppm, MnP 639 ppm, metmyoglobin 930 ppm). The shift

of 612 ppm for MnC*c*P suggests that the heme Fe(III)−N(His) bond in this protein is weaker than that in WtC*c*P (587 ppm), but closer to that in MnP (639 ppm). This is in complete agreement with the less imidazolate character of the proximal histidine suggested by ^{1}H NMR experiments. The observed chemical shift for Hϵ1 of the proximal histidine in MnC*c*PCN is actually comparable to the corresponding proton in MnPCN.

In conclusion, the results presented in this paper demonstrate that successful application of NOESY techniques in conjunction with traditional 1D NOE experiments and examination of the crystal structural parameters for Wt-C*c*PCN can lead to unambiguous assignments for the hyperfine-shifted resonances of this engineered MnC*c*P enzyme. The resonance assignment combined with specific signal broadening by a paramagnetic ion Mn(II) confirms the creation of the single Mn(II)-binding site at the designed location. Furthermore, introduction of this Mn(II) site, although having no detectable impact on the structure of the distal side of the heme, imposes noticeable changes on the pK_a of the heme Fe(III) spin state change and the local structure of the proximal side of the heme, particularly the heme Fe(III)−N(His) bond strength. These results, together with the finding of the existence of two different forms of the protein in solution and their temperature-dependent interconversion, demonstrate the need for structural characterization using NMR to complement X-ray structural analysis.

ACKNOWLEDGMENT

We are grateful to Bryan K. S. Yeung for his initial work on this project, Professor F. Ann Walker and Mr. Alan J. Gengenbach for their helpful discussions, and Angela Kwon for proofreading the manuscript. NMR spectra were obtained in the Varian Oxford Instrument Center for Excellence in NMR Laboratory. Funding for this instrumentation was provided in part from the W. M. Keck Foundation, the National Institutes of Health (PHS 1 S10 RR10444-01), and the National Science Foundation (NSF CHE 96-10502).

SUPPORTING INFORMATION AVAILABLE

Four figures displaying the temperature dependence of the NMR spectra of the resting state of MnC*c*P and COSY and NOESY spectra (in 90% H_2O/10% D_2O and in D_2O only) of MnC*c*PCN (5 pages). This material is available free of charge via the Internet at http://pubs.acs.org.

REFERENCES

1. Everse, J., Everse, K. E., and Grisham, M. B. (1990) *Peroxidases in Chemistry and Biology*, Vol. I, CRC Press, Boca Raton, FL.
2. Welinder, K. G., and Gajhede, M. (1993) *Plant Peroxidases: Biochemistry and Physiology*, University of Geneva Press, Geneva, Switzerland.
3. Poulos, T. L., and Fenna, R. E. (1994) *Met. Ions Biol. Syst. 30*, 25−75.
4. English, A. M., and Tsaprailis, G. (1995) *Adv. Inorg. Chem. 43*, 79−125.
5. Poulos, T. L., and Kraut, J. (1980) *J. Biol. Chem. 255*, 8199−8205.
6. Finzel, B. C., Poulos, T. L., and Kraut, J. (1984) *J. Biol. Chem. 259*, 13027−13036.
7. Edwards, S. L., and Poulos, T. L. (1990) *J. Biol. Chem. 265*, 2588−2595.
8. Edwards, S. L., Raag, R., Wariishi, H., Gold, M. H., and Poulos, T. L. (1993) *Proc. Natl. Acad. Sci. U.S.A. 90*, 750−754.
9. Poulos, T. L., Edwards, S. L., Wariishi, H., and Gold, M. H. (1993) *J. Biol. Chem. 268*, 4429−4440.
10. Sundaramoorthy, M., Kishi, K., Gold, M. H., and Poulos, T. L. (1994) *J. Biol. Chem. 269*, 32759−32767.
11. Gajhede, M., Schuller, D. J., Henriksen, A., Smith, A. T., and Poulos, T. L. (1997) *Nat. Struct. Biol. 4*, 1032−1038.
12. Dawson, J. H. (1988) *Science (Washington, DC.) 240*, 433−439.
13. Poulos, T. L. (1996) *J. Biol. Inorg. Chem. 1*, 356−359.
14. Goodin, D. B. (1996) *J. Biol. Inorg. Chem. 1*, 360−363.
15. Banci, L., Rosato, A., and Turano, P. (1996) *J. Biol. Inorg. Chem. 1*, 364−367.
16. Gross, Z. (1996) *J. Biol. Inorg. Chem. 1*, 368−371.
17. Rietjens, I. M. C. M., Osman, A. M., Veeger, C., Zakharieva, O., Antony, J., Grodzicki, M., and Trautwein, A. X. (1996) *J. Biol. Inorg. Chem. 1*, 372−376.
18. Weiss, R., Mandon, D., Wolter, T., Trautwein, A. X., Muther, M., Bill, E., Gold, A., Jayaraj, K., and Terner, J. (1996) *J. Biol. Inorg. Chem. 1*, 377−383.
19. Gold, M. H., Wariishi, H., and Valli, K. (1989) *ACS Symp. Ser. 389*, 127−140.
20. Cai, D., and Tien, M. (1993) *J. Biotechnol. 30*, 79−90.
21. Stahl, J. D., and Aust, S. D. (1998) *Rev. Toxicol. (Amsterdam) 2*, 189−194.
22. Wariishi, H., Valli, K., and Gold, M. H. (1992) *J. Biol. Chem. 267*, 23688−23695.
23. Mauk, M. R., Kishi, K., Gold, M. H., and Mauk, A. G. (1998) *Biochemistry 37*, 6767−6771.
24. Banci, L., Bertini, I., Bini, T., Tien, M., and Turano, P. (1993) *Biochemistry 32*, 5825−5831.
25. Sundaramoorthy, M., Kishi, K., Gold, M. H., and Poulos, T. L. (1997) *J. Biol. Chem. 272*, 17574−17580.
26. Kishi, K., Kusters-van Someren, M., Mayfield, M. B., Sun, J., Loehr, T. M., and Gold, M. H. (1996) *Biochemistry 35*, 8986−8994.
27. Whitwam, R. E., Brown, K. R., Musick, M., Natan, M. J., and Tien, M. (1997) *Biochemistry 36*, 9766−9773.
28. Bryson, J. W., Betz, S. F., Lu, H. S., Suich, D. J., Zhou, H. X. X., Oneil, K. T., and Degrado, W. F. (1995) *Science 270*, 935−941.
29. Lu, Y., and Valentine, J. S. (1997) *Curr. Opin. Struct. Biol. 7*, 495−500.
30. Yeung, B. K., Wang, X., Sigman, J. A., Petillo, P. A., and Lu, Y. (1997) *Chem. Biol. 4*, 215−221.
31. Bosshard, H. R., Anni, H., and Yonetani, T. (1991) in *Peroxidases in Chemistry and Biology* (Everse, J., Everse, K. E., and Grisham, M. B., Eds.) Vol. II, pp 51−84, CRC Press, Boca Raton, FL.
32. Wilcox, S. K., Putnam, C. D., Sastry, M., Blankenship, J., Chazin, W. J., McRee, D. E., and Goodin, D. B. (1998) *Biochemistry 37*, 16853−16862.
33. Hellinga, H. W. (1996) *Curr. Opin. Biotechnol. 7*, 437−441.
34. Wang, X., and Morden, K. M. (1997) *Methods Mol. Biol. (Totowa, N.J.) 78*, 85−112.
35. Vold, R. L., Waugh, J. S., Klein, M. P., and Phelps, D. E. (1968) *J. Chem. Phys. 48*, 3831−3832.
36. States, D. J., Haberkorn, R. A., and Ruben, D. J. (1982) *J. Magn. Reson. 48*, 286−292.
37. Ferrer, J. C., Turano, P., Banci, L., Bertini, I., Morris, I. K., Smith, K. M., Smith, M., and Mauk, A. G. (1994) *Biochemistry 33*, 7819−7829.
38. Turano, P., Ferrer, J. C., Cheesman, M. R., Thomson, A. J., Banci, L., Bertini, I., and Mauk, A. G. (1995) *Biochemistry 34*, 13895−13905.
39. Satterlee, J. D., Erman, J. E., Mauro, J. M., and Kraut, J. (1990) *Biochemistry 29*, 8797−8804.
40. La Mar, G. N. (1979) in *Biological Applications of Magnetic Resonance* (Shulman, R. G., Ed.) pp 305−343, Academic Press, New York.

41. Satterlee, J. D. (1986) in *Annual reports on NMR spectroscopy* (Webb, G. A., Ed.) Vol. 17, pp 79−178, Academic Press, London.
42. Satterlee, J. D., Erman, J. E., LaMar, G. N., Smith, K. M., and Langry, K. C. (1983) *Biochim. Biophys. Acta 743*, 246−255.
43. Smulevich, G., Feis, A., Indiani, C., Becucci, M., and Marzocchi, M. P. (1999) *J. Biol. Inorg. Chem. 4*, 39−47.
44. Banci, L., Bertini, I., Turano, P., Ferrer, J. C., and Mauk, A. G. (1991) *Inorg. Chem. 30*, 4510−4516.
45. Bertini, I., and Luchinat, C. (1986) *NMR of Paramagnetic Molecules in Biological Systems*, Benjamin/Cummings, Menlo Park, CA.
46. De Ropp, J. S., Yu, L. P., and La Mar, G. N. (1991) *J. Biomol. NMR 1*, 175−190.
47. La Mar, G. N., and de Ropp, J. S. (1993) in *NMR of Paramagnetic Molecules* (Berliner, L. J., and Reuben, J., Eds.) Vol. 12, pp 1−78, Plenum Press, New York.
48. La Mar, G. N., Chen, Z., Vyas, K., and McPherson, A. D. (1995) *J. Am. Chem. Soc. 117*, 411−419.
49. Satterlee, J. D., Erman, J. E., LaMar, G. N., Smith, K. M., and Langry, K. C. (1983) *J. Am. Chem. Soc. 105*, 2099−2104.
50. Satterlee, J. D., Erman, J. E., and DeRopp, J. S. (1987) *J. Biol. Chem. 262*, 11578−11583.
51. Thanabal, V., De Ropp, J. S., and La Mar, G. N. (1987) *J. Am. Chem. Soc. 109*, 7516−7525.
52. Dugad, L. B., Wang, X., Wang, C. C., Lukat, G. S., and Goff, H. M. (1992) *Biochemistry 31*, 1651−1655.
53. Dugad, L. B., and Goff, H. M. (1992) *Biochim. Biophys. Acta 1122*, 63−69.
54. Bertini, I., Turano, P., and Vila, A. J. (1993) *Chem. Rev. (Washington, D.C.) 93*, 2833−2932.
55. La Mar, G. N., and Walker, F. A. (1979) in *Porphyrins* (Dolphin, D., Ed.) pp 61−157, Academic Press, New York.
56. Walker, A. F., and Simonis, U. (1993) in *NMR of Paramagnetic Molecules* (Berliner, L. J., and Reuben, J., Eds.) Vol. 12, pp 133−274, Plenum Press, New York.
57. Satterlee, J. D., and Erman, J. E. (1991) *Biochemistry 30*, 4398−4405.
58. Banci, L., Bertini, I., Pease, E. A., Tien, M., and Turano, P. (1992) *Biochemistry 31*, 10009−10017.
59. Banci, L., Bertini, I., Kuan, I. C., Tien, M., Turano, P., and Vila, A. J. (1993) *Biochemistry 32*, 13483−13489.
60. Thanabal, V., De Ropp, J. S., and La Mar, G. N. (1988) *J. Am. Chem. Soc. 110*, 3027−3035.
61. Satterlee, J. D., Russell, D. J., and Erman, J. E. (1991) *Biochemistry 30*, 9072−9077.
62. Thanabal, V., DeRopp, J. S., and La Mar, G. N. (1987) *J. Am. Chem. Soc. 109*, 265−272.
63. La Mar, G. N., and De Ropp, J. S. (1979) *Biochem. Biophys. Res. Commun. 90*, 36−41.
64. Shokhirev, N. V., and Walker, F. A. (1998) *J. Biol. Inorg. Chem. 3*, 581−594.
65. Shokhirev, N. V., and Walker, F. A. (1998) *J. Am. Chem. Soc. 120*, 981−990.
66. Aguiar, A. P., Costa, H. S., Louro, R. O., Xavier, A. V., and Turner, D. L. (1998) *Inorg. Chim. Acta 273*, 196−200.
67. Louro, R. O., Correia, I. J., Brennan, L., Coutinho, I. B., Xavier, A. V., and Turner, D. L. (1998) *J. Am. Chem. Soc. 120*, 13240−13247.
68. Edwards, S. L., Kraut, J., and Poulos, T. L. (1988) *Biochemistry 27*, 8074−8081.
69. Banci, L., Bertini, I., Turano, P., Tein, M., and Kirk, T. K. (1991) *Proc. Natl. Acad. Sci. U.S.A. 88*, 6956−6960.
70. De Ropp, J. S., La Mar, G. N., Wariishi, H., and Gold, M. H. (1991) *J. Biol. Chem. 266*, 15001−15008.
71. Thanabal, V., and La Mar, G. N. (1989) *Biochemistry 28*, 7038−7044.
72. Chen, Z., de Ropp, J. S., Hernandez, G., and La Mar, G. N. (1994) *J. Am. Chem. Soc. 116*, 8772−8783.
73. Wuthrich, K. (1986) *NMR of Proteins and Nucleic Acids*, John Wiley & Sons, New York.
74. Behere, D. V., Gonzalez-Vergara, E., and Goff, H. M. (1985) *Biochim. Biophys. Acta 832*, 319−325.
75. Morishima, I., Inubushi, T., Neya, S., Ogawa, S., and Yonezawa, T. (1977) *Biochem. Biophys. Res. Commun. 78*, 739−746.
76. Morishima, I., and Inubushi, T. (1977) *J. Chem. Soc., Chem. Commun.*, 616−617.
77. Morishima, I., and Inubushi, T. (1978) *J. Am. Chem. Soc. 100*, 3568−3574.
78. Shiro, Y., Iizuka, T., Makino, R., Ishimura, Y., and Morishima, I. (1989) *J. Am. Chem. Soc. 111*, 7707−7711.
79. Vitello, L. B., Huang, M., and Erman, J. E. (1990) *Biochemistry 29*, 4283−4288.
80. Smulevich, G., Miller, M. A., Kraut, J., and Spiro, T. G. (1991) *Biochemistry 30*, 9546−9558.
81. Krishnamoorthi, R., La Mar, G. N., Mizukami, H., and Romero, A. (1984) *J. Biol. Chem. 259*, 265−270.
82. McGrath, T. M., and La Mar, G. N. (1978) *Biochim. Biophys. Acta 534*, 99−111.
83. Antonini, E., and Brunori, M. (1971) *Hemoglobin and Myoglobin in their Reactions with Ligands (Frontiers of Biology, Vol. 21)*, Elsevier, New York.
84. Satterlee, J. D., Alam, S. L., Mauro, J. M., Erman, J. E., and Poulos, T. L. (1994) *Eur. J. Biochem. 224*, 81−87.
85. Alam, S. L., Satterlee, J. D., Mauro, J. M., Poulos, T. L., and Erman, J. E. (1995) *Biochemistry 34*, 15496−15503.

BI990235R